Ultrasonics 77 (2017) 100–109

Contents lists available at ScienceDirect

Ultrasonics

journal homepage: www.elsevier.com/locate/ultras

Propagation of thickness shear waves in a periodically corrugated quartz crystal plate and its application exploration in acoustic wave filters

Peng Li [a,b], Li Cheng [a,*]

[a] Department of Mechanical Engineering, Hong Kong Polytechnic University, Hong Kong, PR China
[b] School of Human Settlements and Civil Engineering, Xi'an Jiaotong University, Xi'an 710049, PR China

ARTICLE INFO

Article history:
Received 23 September 2016
Received in revised form 12 January 2017
Accepted 4 February 2017
Available online 7 February 2017

Keywords:
Phononic quartz crystal plate
Thickness shear waves
Power series expansion
Energy trapping
Acoustic wave filter

ABSTRACT

The propagation of thickness shear waves in a periodically corrugated quartz crystal plate is investigated in the present paper using a power series expansion technique. In the proposed simulation model, an equivalent continuity of shear stress moment is introduced as an approximation to handle sectional interfaces with abrupt thickness changes. The Bloch theory is applied to simulate the band structures for three different thickness variation patterns. It is shown that the power series expansion method exhibits good convergence and accuracy, in agreement with results by finite element method (FEM). A broad stop band can be obtained in the power transmission spectra owing to the trapped thickness shear modes excited by the thickness variation, whose physical mechanism is totally different from the well-known Bragg scattering effect and is insensitive to the structural periodicity. Based on the observed energy trapping phenomenon, an acoustic wave filter is proposed in a quartz plate with sectional decreasing thickness, which inhibits wave propagation in different regions.

1. Introduction

Elastic wave propagation in periodic structures has been receiving increasing attention over the past decade. With multiple periodic constituents, these structures, referred to as phononic crystals (PCs), exhibit unique physical properties such as complete band gaps (BGs) which prohibits elastic wave propagation and the possibility for manipulating wave traveling paths. Owing to these features, PCs are proposed as promising candidates for conceiving acoustic devices, such as acoustic filters, directional acoustic wave sources, silent blocks and waveguides etc. [1–5]. Generally speaking, two well-established physical mechanisms result in the formation of the band gaps, known as the Bragg scattering [1,2] and the local resonances [3,4]. The former is resulted from the periodicity of the structure; the latter, however, depends less on the structural periodicity, which allows the creation of the BG which can be almost two orders of magnitude lower than that from Bragg scattering effect.

A growing number of investigations have been carried out on the design and application of PCs through theoretical, numerical and experimental means [1–8]. Impedance mismatch existing in the wave propagation path is the intrinsic reason behind the formation of the BGs, which can be artificially designed by arranging and tuning mass densities and elastic coefficients periodically in space. Besides, the mismatched impedance can also be achieved through varying the structural shape or geometry parameters [9–14]. For example, an infinite phononic crystal beam or plate with periodic thickness variations can also give rise to BGs [15–18], whose broadband efficiency can be controlled by adjusting thickness variation [15–17]. Meanwhile, other remarkable dispersion properties, such as zero group velocity, negative group refraction index, bi-refraction etc., can also be found in a PC with one single material component [18]. Periodically corrugated structures provide a potential substitution for wave devices, since less parameters are involved (only thickness of unit cell). This makes the design and manufacturing extremely simple and convenient, avoiding the requirement on multi-phase material or resonant structures used in the conventional approach.

Material-wise, quartz is one of the most widely used crystals in acoustic devices because of its high temperature and frequency stability. A large portion of quartz resonant devices operate under the so-called thickness-shear vibration mode, whose frequencies depend on thickness [19,20]. It can be surmised that a phononic quartz crystal plate with non-uniform thickness would greatly impact on the propagation of thickness shear waves. Meanwhile, along with the existence of the band gap, the energy trapping phenomenon, which is crucial to device mounting, would also take

* Corresponding author.
E-mail address: li.cheng@polyu.edu.hk (L. Cheng).

http://dx.doi.org/10.1016/j.ultras.2017.02.004
0041-624X/

place due to thickness variation [21,22]. When that happens, waves at particular frequencies cannot propagate freely. It is therefore important to investigate the distinction and relation between the band gap and energy trapping phenomenon in view of design of acoustic wave devices.

In the present paper, we investigate the propagation of thickness shear waves in a periodically corrugated quartz crystal plate. A general model, along with solution procedure, is proposed, which is capable of dealing with plate thickness changes described by an arbitrary function. This is different from the previous work considering either flat [16,23,24] or some specific thickness profiles such as hyperbolic [21] or quadratic [24]. Based on the model, a power series expansion technique is proposed to obtain the semi-analytical solution, whose validity is assessed through comparison with FEM results. Upon generating the frequency spectra, broad stop bands caused by energy trapping phenomenon are analyzed in detail and compared with Bragg scattering effect. At last, based on the trapped thickness shear modes, an acoustic wave filter with frequency-dependent wave trapping and separation capability is designed.

2. Modelling of the thickness shear waves in a periodic quartz crystal plate

A periodically corrugated AT-cut quartz plate occupying the region $0 \leqslant x_3 \leqslant D$, shown in Fig. 1(a), is considered. The plate is subject to a thickness (x_2 direction) shear waves coming from $x_3 < 0$. The widely used AT-cut quartz plate is a special case of the rotated Y-cut quartz plate that is effectively monoclinic. The corrugated plate is composed of a series of unit cells with a length L shown in Fig. 1(b), whose thickness variation can be described by a slowly varying function $h = h(x_3)$. $h(x_3)$ can either be a known function for a given profile or an unknown function to be determined in order to obtain the desired wave-stop effect. It is obvious that the corrugation leads to mismatched acoustic impedance, similar in effect but different in mechanism from the staggered arrangement in mass densities or elastic coefficients.

Because of the complexity associated with the material anisotropy of the quartz and thickness variation, exact solution of the thickness shear waves can hardly be obtained. For AT-cut quartz plates, however, the only one dominating displacement component $u_1 = u_1(x_2, x_3, t)$ controlling the anti-plane vibration can be approximated as the sum of different anti-symmetric modes in x_2 direction as [16,23–26]

$$u_2 = u_3 = 0, \quad u_1 = u_1(x_2, x_3, t) = \sum_{n=1,3,5}^{\infty} U^{(n)}(x_3, t) \sin\frac{n\pi x_2}{2h(x_3)} \tag{1}$$

where, u_i (i = 1, 2, 3) stands for the particle displacement; t is the time and $2h(x_3)$ the thickness of quartz plate. n = 1 represents the fundamental family of modes, and n > 1 belongs to the case of overtone modes. For crystal resonators and filters, u_1 is anti-symmetric about the plate middle plane at x_2 = 0, due to the fact that anti-plane vibration is the predominant component that can be excited by an electric field along the plate thickness direction. Based on the assumption that the unit cell has a slow varying contour, the governing equation in terms of $U^{(n)}$ can be written as [26,21]

$$c_{55}\frac{\partial^2 U^{(n)}}{\partial x_3^2} - \frac{n^2\pi^2}{4h^2(x_3)}\bar{c}_{66}U^{(n)} - \rho\frac{\partial^2 U^{(n)}}{\partial t^2} = 0 \tag{2}$$

where c_{55} and $\bar{c}_{66}$ are the effective elastic parameters and ρ the mass density of the quartz plate. In this particular case, c_{55} = 68.81 GPa and $\bar{c}_{66} = \left(c_{66} + \frac{e_{26}^2}{\varepsilon_{22}}\right)\left(1 - \frac{8k_{26}^2}{\pi^2}\right)$. Here, e_{26}, $_{22}$ and k_{26}^2 are respectively piezoelectric and dielectric constants and mechanical-electrical coupling factor of quartz plate [21,23,26]. The detailed derivation process of Eq. (2) can be found in the work by Tiersten [23,26], in which weak piezoelectric coupling and small unimportant elastic constants (c_{14}, c_{25} and c_{56}) have been ignored for simplification. In harmonic regime, $U^{(n)}(x_3, t) = U^{(n)}(x_3)\exp(-i\omega t)$. Eq. (2) retreats to:

$$\frac{h^2(x_3)}{h_0^2}\frac{d^2U^{(n)}(x_3)}{dx_3^2} + \left[\frac{\omega^2}{c_{55}/\rho}\frac{h^2(x_3)}{h_0^2} - \frac{n^2\pi^2}{4h_0^2}\frac{\bar{c}_{66}}{c_{55}}\right]U^{(n)}(x_3) = 0 \tag{3}$$

$h(x_3)$ can be expressed in terms of power function using Taylor's series expansion, so that

$$h^2(x_3) = h_0^2\sum_{m=0,1,2,}^{\infty} H_m\left(\frac{x_3}{L}\right)^m \tag{4}$$

where h_0 is the half thickness at x_3 = 0; and H_m the coefficients determining $h(x_3)$. Similarly, Eq. (3) can be solved by seeking approximate solutions through polynomial expansion as [27–29]

$$U^{(n)}(x_3) = \sum_{m=0,1,2,}^{\infty} A_m^{(n)}\left(\frac{x_3}{L}\right)^m \tag{5}$$

where $A_m^{(n)}$ is the unknown coefficient to be determined. Substituting Eqs. (4) and (5) into Eq. (3) yields:

$$\sum_{s=0,1,2,}^{\infty} H_s\left(\frac{x_3}{L}\right)^s \sum_{m=0,1,2,}^{\infty}(m+2)(m+1)A_{m+2}^{(n)}\left(\frac{1}{L}\right)^2\left(\frac{x_3}{L}\right)^m + \left[\frac{\omega^2}{c_{55}/\rho}\sum_{s=0,1,2,}^{\infty} H_s\left(\frac{x_3}{L}\right)^s - \frac{n\pi^2}{4h_0^2}\frac{\bar{c}_{66}}{c_{55}}\right]\sum_{m=0,1,2,}^{\infty} A_m^{(n)}\left(\frac{x_3}{L}\right)^m = 0 \tag{6}$$

By equating the coefficients of $\left(\frac{x_3}{L}\right)^m$ in above equation to zero, one obtains:

$$\sum_{s=0,1,2,}^{m} H_s(m+2-s)(m+1-s)A_{m+2-s}^{(n)} + \frac{\omega^2 L^2}{c_{55}/\rho}\sum_{s=0,1,2,}^{m} H_s A_{m-s}^{(n)} - \frac{n\pi^2 L^2}{4h_0^2}\frac{\bar{c}_{66}}{c_{55}}A_m^{(n)} = 0 \tag{7}$$

Eq. (7) describes a series of linear recursive relations for $A_m^{(n)}$ with m changing from zero to infinity, which provides much convenience for the numerical calculation. In an explicit form:

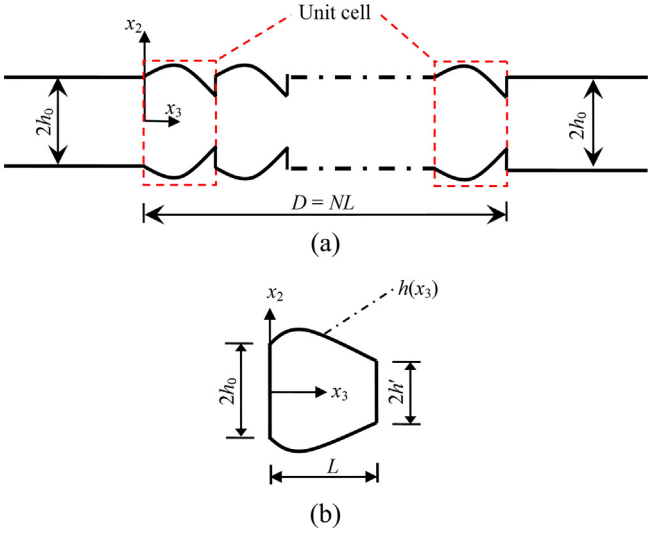

Fig. 1. Theoretical model: (a) an AT-cut corrugated quartz crystal plate; (b) a unit cell.

$$
\begin{aligned}
A_2^{(n)} &= -\frac{L^2}{2}\frac{n\pi^2}{4h_0^2}\frac{\bar{c}_{66}}{c_{55}}\left(\Omega^2-\frac{1}{H_0}\right)A_0^{(n)},\\
A_3^{(n)} &= -\frac{H_1}{3H_0}A_2^{(n)}-\frac{L^2}{6}\frac{n\pi^2}{4h_0^2}\frac{\bar{c}_{66}}{c_{55}}\left[\Omega^2\left(A_1^{(n)}+\frac{H_1}{H_0}A_0^{(n)}\right)-\frac{1}{H_0}A_1^{(n)}\right],\\
A_4^{(n)} &= -\frac{H_1}{2H_0}A_3^{(n)}-\frac{H_2}{6H_0}A_2^{(n)}\\
&\quad -\frac{L^2}{12}\frac{n\pi^2}{4h_0^2}\frac{\bar{c}_{66}}{c_{55}}\left[\Omega^2\left(A_2^{(n)}+\frac{H_1}{H_0}A_1^{(n)}+\frac{H_2}{H_0}A_0^{(n)}\right)-\frac{1}{H_0}A_2^{(n)}\right],\\
&\cdots
\end{aligned}
\tag{8}
$$

where $\Omega=\frac{\omega}{\omega_s}$ with $\omega_s=\frac{n\pi}{2h_0}\sqrt{\frac{\bar{c}_{66}}{\rho}}$ being the cut-off frequency (to be explained in detail below). It can be seen from Eq. (8) that the first two coefficients $A_0^{(n)}$ and $A_1^{(n)}$ are to be determined first, after which $A_m^{(n)}$ with $m>1$ can be successively obtained using Eq. (7).

For a unit cell in a periodic quartz plate, shown in Fig. 1(b), the mismatched thickness at $x_3=0$ and L leads to the difficulty of satisfying the exact displacement and stress continuity. Instead, we impose the continuity of the moment of shear stress at the interface as an approximation [16]. Meanwhile, the Bloch theorem is applied for the boundary conditions at $x_3=0$ and L:

$$
\begin{cases}
U^{(n)}(0)=U^{(n)}(L)e^{-iKL}\\
\int_{-h(0)}^{h(0)} c_{55}\frac{dU^{(n)}(0)}{dx_3}x_2\sin\frac{n\pi x_2}{2h(0)}dx_2=\int_{-h(L)}^{h(L)} c_{55}\frac{dU^{(n)}(L)}{dx_3}x_2\sin\frac{n\pi x_2}{2h(L)}dx_2e^{-iKL}
\end{cases}
\tag{9}
$$

where K is the wavenumber, real in certain frequency ranges and strictly imaginary in others, whose value is restricted within the first Brillouin zone. In general, K can be written as $K=\mathrm{Real}(K)+i\mathrm{Imag}(K)$. If K is real with its value changing in the half of the first Brillouin zone region $[0, L/\pi]$, displacement and stress at positions $x_3=0$ and $x_3=L$ differ only by a phase factor $e^{i\mathrm{Real}(K)L}$. This indicates that waves can travel, thus forming frequency pass bands. On the contrary, if K is imaginary, i.e., there will be a spatial exponential attenuation in magnitude of displacement and stress when waves propagate across the unit. As a result, waves in these frequency ranges are effectively prohibited from traveling to long distance, thus forming frequency stop bands.

Substituting Eq. (5) into the boundary condition above yields two linear, homogeneous algebraic equations in terms of $A_0^{(n)}$ and $A_1^{(n)}$, i.e.,

$$
\begin{cases}
\sum_{m=0,1,2,}^{\infty} A_m^{(n)}e^{-iKL}-A_0^{(n)}=0\\
\sum_{m=0,1,2,}^{\infty}\frac{h'^2}{h_0^2}(m+1)A_{m+1}^{(n)}e^{-iKL}-A_1^{(n)}=0
\end{cases}
\tag{10}
$$

Non-trivial solutions exist only when the determinant of the coefficient matrix of Eq. (10) is equal to zero, from which we can get the dispersion curve for the infinite periodic quartz crystal plate.

3. Numerical simulations on periodic quartz crystal plates

Eq. (10) is a transcendental equation wherein the wavenumber K and non-dimensional frequency Ω cannot be obtained directly using an explicit expression. Therefore, a suitable computation method should be developed to solve the problem. For a given Ω, the roots of Eq. (10), i.e., the values of K locating in the region of $[0, L/\pi]$, are to be determined. The K-space, whose real and imaginary parts are respectively limited in the region of $[-\delta, \delta+L/\pi]$ and $[-\delta, \delta+\mu L/\pi]$ (with μ being a real positive number, standing for the decaying rate of amplitude), is divided into finite meshes by a small step, and each cross point possesses individual K value. Here, the solving area has been enlarged by a small amount in order to account for the case of $K=0$ and $K=L/\pi$. Then, we calculate the determinant value of Eq. (10) in every cross point for each given frequency Ω. Any point whose absolute value of determinant is smaller than the other eight ones in the neighborhood will be considered as the final root. In the present case, the evanescent wave caused by Bragg scattering effect is of interest, which has the weakest attenuation during its propagation. Hence, μ should be chosen appropriately during every iteration process so that there is only one root in the targeted solving region.

The convergence of the power series method is first examined, by setting $2h_0=5$ mm and $L=20$ mm for one unit, with $n=1$. For verification and comparison purposes, we consider three cases corresponding to three different thickness profiles, respectively: linear, quadratic and stepped functions, defined as:

$$
\mathrm{Case1}:\ \frac{h(x_3)}{h_0}=1-\frac{1}{2}\left(\frac{x_3}{L}\right)
\tag{11a}
$$

$$
\mathrm{Case2}:\ \frac{h(x_3)}{h_0}=1-\frac{1}{8}\left(\frac{x_3}{L}\right)-\frac{3}{8}\left(\frac{x_3}{L}\right)^2
\tag{11b}
$$

$$
\mathrm{Case3}:\ \frac{h(x_3)}{h_0}=\begin{cases}1.0, & 0\leqslant x_3\leqslant 0.5L\\ 0.5, & 0.5L\leqslant x_3\leqslant L\end{cases}
\tag{11c}
$$

Note that the thickness of all unit cells at $x_3=L$ equals to h_0, shown in Fig. 2. It is relevant to note that, for Case 3, two individual power series should be used separately for $0\leqslant x_3\leqslant 0.5L$ and $0.5L\leqslant x_3\leqslant L$, to ensure the corresponding displacement and shear stress moment continuity at the interface $x_3=0.5L$. Tables 1–3 show the convergence of the calculation for the three cases, with different truncations used in the power function expansion, respectively. It can be seen that the convergence is achieved in each case, but convergence feature is closely related to the frequency and thickness variation pattern. More terms are required for linear and quadratic profiles than the stepped function case, especially for the higher frequencies. Based on this, 40 terms are deemed sufficient to achieve acceptable accuracy for the stepped variation pattern and 80 terms will be used for the linear and quadratic variation functions in the following simulations.The frequency spectrum calculated from Eq. (10) for the three cases is shown in Fig. 3. Meanwhile, results using Finite Element Method with periodic boundary conditions using Comsol Multiphysics software are also given, denoted by black circles. The abscissa is the non-dimensional wave number KL/π, ranging from 0 to 1, representing the first Brillouin zone (the region $[-1,0]$ is symmetric with that of $[0,1]$). Results from the power function expansion technique are largely in good agreement with the FEM ones, thus validating the established model and numerical procedure to some

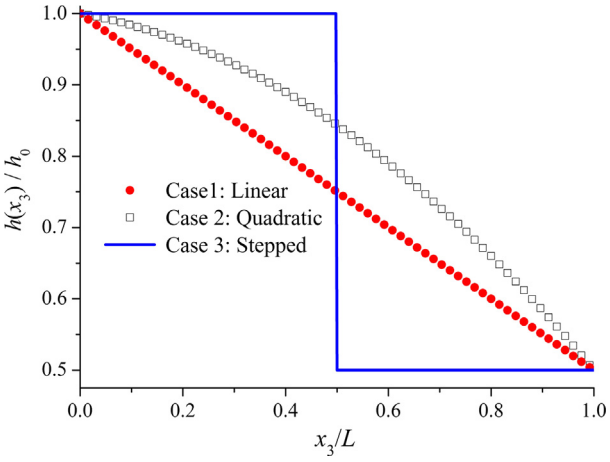

Fig. 2. Three thickness profiles of the quartz unit cell.

Table 1
K values calculated by the power function expansion method for selected frequencies with thickness changes in Case 1.

$\left(\frac{\mathrm{Real}(K)L}{\pi}, \frac{\mathrm{Imag}(K)L}{\pi}\right)$	$M = 50$	$M = 60$	$M = 70$	$M = 80$
$\Omega = 1.0$	(0, 2.4518)	(0, 2.4518)	(0, 2.4518)	(0, 2.4518)
$\Omega = 1.25$	(0, 0.93184)	(0, 0.93184)	(0, 0.93184)	(0, 0.93184)
$\Omega = 1.5$	(1.0, 0.24232)	(1.0, 0.24232)	(1.0, 0.24232)	(1.0, 0.24232)
$\Omega = 1.75$	(0.583, 0)	(0.583, 0)	(0.583, 0)	(0.583, 0)
$\Omega = 2.0$	(0.3885, 0)	(0.3885, 0)	(0.3885, 0)	(0.3885, 0)
$\Omega = 2.25$	(0.5055, 0)	(0.506, 0)	(0.506, 0)	(0.506, 0)
$\Omega = 2.5$	(0.616, 0.00416)	(0.6715, 0)	(0.6715, 0)	(0.6715, 0)
$\Omega = 2.75$	(0, 0.06396)	(0.103, 0.000520)	(0.1025, 0)	(0.1025, 0)
$\Omega = 3.0$			(0.8695, 0)	(0.8695, 0)

Table 2
K values calculated by the power function expansion method for selected frequencies with thickness changes in Case 2.

$\left(\frac{\mathrm{Real}(K)L}{\pi}, \frac{\mathrm{Imag}(K)L}{\pi}\right)$	$M = 50$	$M = 60$	$M = 70$	$M = 80$
$\Omega = 1.0$	(0, 2.003)	(0, 2.003)	(0, 2.003)	(0, 2.003)
$\Omega = 1.25$	(1.0, 0.9644)	(1.0, 0.9644)	(1.0, 0.9644)	(1.0, 0.9644)
$\Omega = 1.5$	(0, 0.5)	(0, 0.5)	(0, 0.5)	(0, 0.5)
$\Omega = 1.75$	(1.0, 0.25)	(1.0, 0.25)	(1.0, 0.25)	(1.0, 0.25)
$\Omega = 2.0$	(0, 0.0772)	(0, 0.0772)	(0, 0.0772)	(0, 0.0772)
$\Omega = 2.25$	(0.743, 0)	(0.743, 0)	(0.743, 0)	(0.743, 0)
$\Omega = 2.5$		(0.4785, 0)	(0.4785, 0)	(0.4785, 0)
$\Omega = 2.75$			(0.274, 0)	(0.274, 0)
$\Omega = 3.0$		(1.0, 0.37)	(1.0, 0.0348)	(1.0, 0.035)

Table 3
K values calculated by the power function expansion method for selected frequencies with thickness changes in Case 3.

$\left(\frac{\mathrm{Real}(K)L}{\pi}, \frac{\mathrm{Imag}(K)L}{\pi}\right)$	$M = 10$	$M = 20$	$M = 30$	$M = 40$
$\Omega = 1.0$	(0, 2.439)	(0, 2.4525)	(0, 2.4525)	(0, 2.4525)
$\Omega = 1.25$	(1.0, 2.038)	(1.0, 2.045)	(1.0, 2.045)	(1.0, 2.045)
$\Omega = 1.5$	(0, 1.7855)	(0, 1.8215)	(0, 1.8215)	(0, 1.8215)
$\Omega = 1.75$	(0, 2.4705)	(0, 1.4925)	(0, 1.4925)	(0, 1.4925)
$\Omega = 2.0$	(1.0, 0.9905)	(1.0, 0.9295)	(1.0, 0.9305)	(1.0, 0.9305)
$\Omega = 2.25$	(1.0, 0.037)	(0, 0.603)	(0, 0.6045)	(0, 0.6045)
$\Omega = 2.5$		(0, 0.092)	(0.899, 0)	(0.899, 0)
$\Omega = 2.75$	(1.0, 0.2305)	(0, 0.27)	(0, 0.471)	(0, 0.471)
$\Omega = 3.0$	(1.0, 0.505)	(1.0, 0.236)	(0.452, 0)	(0.452, 0)

extent. Discrepancies are also noticeable, especially for Case 3, due to the use of approximate boundary condition, i.e., the second equation in Eq. (9) in the theoretical model. The equivalent continuity of shear stress moment obviously affects the region $|h_0 - h'| \leqslant |x_2| \leqslant |h_0|$. Nevertheless, the agreement between the two sets of results is still acceptable.

The non-linear profile of the curves in Fig. 3 shows the dispersive feature of the wave. Frequencies corresponding to real-valued wavenumbers are associated with the pass-band modes, and frequencies matching complex or pure imaginary wavenumbers are associated with stop-band modes. Some complete band gaps caused by the thickness changes appear in different cases, which can be seen in Fig. 3. The beginning and termination of the pass-bands or stop-bands all initiate at the edge of the first Brillouin zone, i.e., $KL/\pi = 0$ or 1. It can be surmised that the stepped variation pattern is more beneficial for the formation of complete band gap compared with the linear and quadratic functions. This is understandable since an abrupt thickness variation generates more significant impedance mismatch at interfaces, thus creating more complex wave reflections and interactions. On the other hand, some flat modes emerge in Fig. 3, for instance, the first three modes with $\Omega < 2$ in Case 3, corresponding to quasi-zero group or energy velocity of the waves. As a result, energy is trapped in some regions of the unit cell. Generally speaking, a relative larger band gap with $\Omega > 2$, caused by Bragg scattering effect, can be obtained by adjusting the material or structural parameters of a unit cell, such as the mass density, elastic coefficient, variation function of thickness, the length of unit cell and so on. In what follows, we will focus on the physical explanation about these flat modes with $\Omega < 2$ and explore application potentials.

>To further demonstrate the existence of the frequency band gaps opened by corrugation, the reflection and transmission power spectra through a finite structure comprising ten unit cells with different thickness variations are calculated, i.e., $N = 10$ in Fig. 1 (a). The transfer matrix method is adopted here to calculate the transmission properties. In the region $x_3 < 0$, $U^{(1)}(x_3, t) = [1 \exp(ik_0 x_3) + r \exp(-ik_0 x_3)] \exp(-i\omega t)$ for a given incident wave of amplitude 1. r then stands for the amplitude of reflected wave, and k_0 is the wavenumber, which can be calculated from Eq. (3). The power series are used to describe the solution for every unit cell in the region of $0 < x_3 < D$. After ten unit cells, the displacement field writes $U^{(1)}(x_3, t) = t \exp(ik_0 x_3) \exp(-i\omega t)$ with t being the amplitude of transmitted wave. By utilizing the continuity of displacement and the moment of shear stress at the interfaces between adjacent units, the relationship about undetermined coefficients can be numerically established. Finally, r and t can be solved through the established transfer matrix model. Hence, the reflection and transmission coefficients can be respectively defined as the energy ratios of the reflected and transmitted waves to the incident wave by $|r|^2$ and $|t|^2$. By varying the excitation frequency

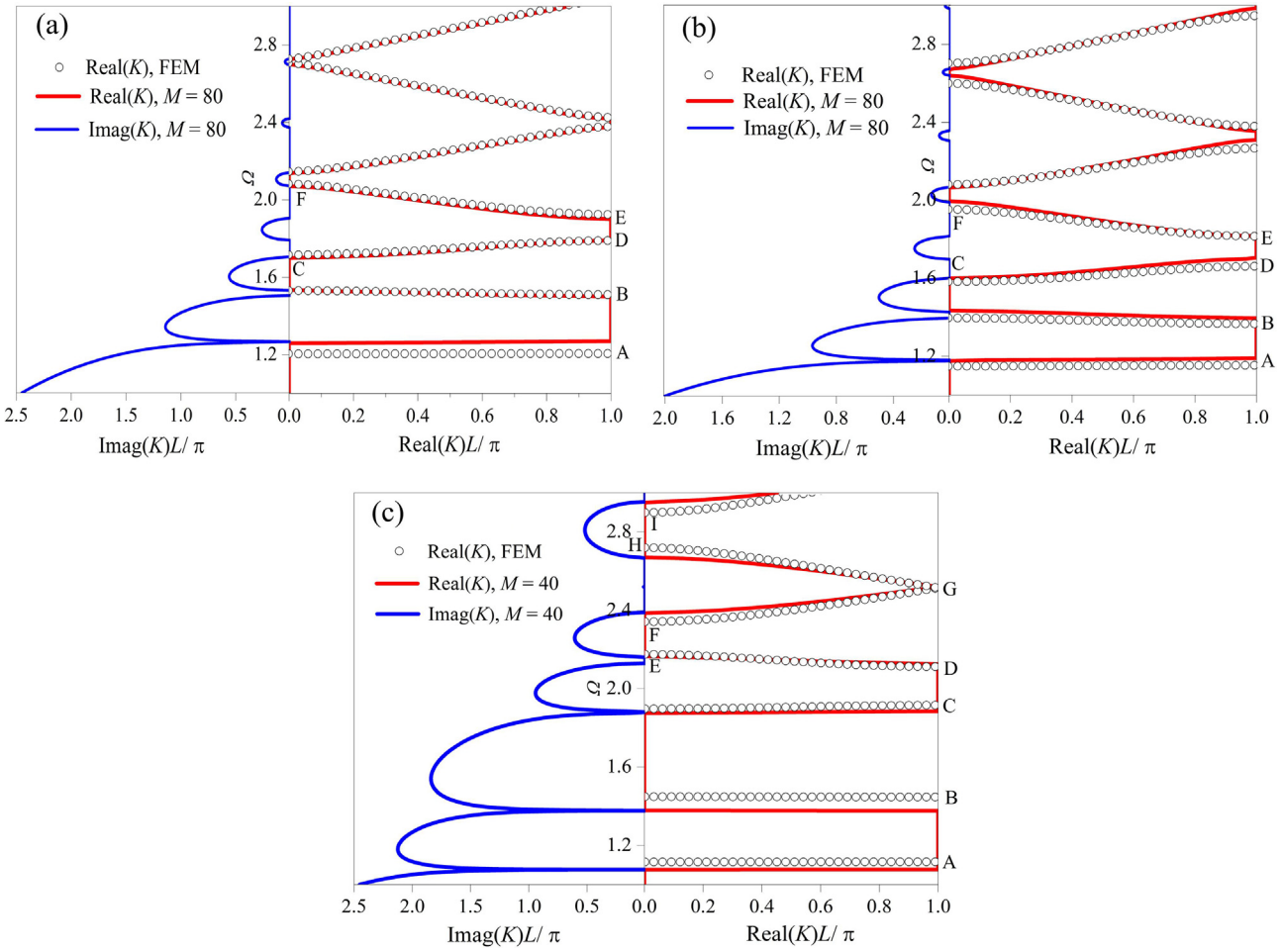

Fig. 3. Frequency spectrum of an infinite periodic quartz crystal plate with the thickness of unit cell changing in the form of: (a) Case 1; (b) Case 2; (c) Case 3.

of the incident wave, the reflection and transmission spectra can be obtained for the three cases above, shown in Fig. 4. The principle of energy conservation stipulates $|r|^2 + |t|^2 = 1$, which also provides the verification of the numerical results. $|r|^2 = 1$ or $|t|^2 = 0$ represents the location of stop bands, which match very well with the results predicted using power series expansion method in Fig. 3 when the thickness of the unit cell changes either linearly or quadratically, even though the transmitted energy of the first mode for Case 1 is rather low. However, for Case 3 with abrupt thickness change, the first three modes cannot be obtained from the reflection and transmission spectra. $|t|^2 = 0$ and $|r|^2 = 1$ in Fig. 4(c) when $\Omega < 2$ indicate the first three modes cannot propagate through the structure with energy totally reflected.

To further explain the disappearance of the first three modes in the reflection and transmission spectra, we calculated the corresponding displacement field of eigenmodes exported by Comsol Multiphysics at several gap-edge frequencies marked in Fig. 3, with results shown in Fig. 5. It can be seen that, Cases 1 and 2 have similar displacement field. The energy mainly focuses on the thicker region of the unit cell for the first mode, gradually extends towards to the thinner region for higher modes. For Case 3, the phenomenon of energy concentration is the most evident. For modes with $\Omega < 2$, the energy in the thicker part is larger than that in the thinner one, especially for the lowest mode. For modes D and E, the vibration is mainly concentrated at the thinner part rather than the thicker one. With the increasing resonance frequency, the energy of higher modes is spread out over the entire unit.

The displacement component of the plate with uniform thickness can be obtained from Eq. (3) as:

$$U^{(1)}(x_3, t) = [A' \exp(ik'x_3) + B' \exp(-ik'x_3)] \exp(-i\omega t) \tag{12}$$

with $k' = \frac{\pi}{2h_0}\sqrt{\frac{\bar{c}_{66}}{c_{55}}\left(\Omega^2 - \frac{h_0^2}{h'^2}\right)}$ representing the wavenumber. A' and B' correspond to the waves propagating in the positive and negative directions of x_3-axis, respectively. The cut-off frequency, Ω_c or ω_s, can be deduced when the wavenumber $k' = 0$. For example, $\Omega_c = 2$ when $h' = 0.5h_0$. If the frequency of incident wave is larger than Ω_c, the wavenumber is real meaning that the wave can propagate freely. Otherwise, k' will become pure imaginary, which leads to the decaying wave amplitude and finally lower the energy transmitted. This results in the energy trapping phenomenon, observed in Fig. 4(c). Larger absolute value of pure imaginary k' makes the energy trapping phenomenon more evident, which can be used to explain the vibration energy concentration comparison marked by A, B and C in Fig. 5(c).

In order to further prove the physical mechanism of the trapped thickness shear modes in the phononic crystal plate, the transmission power spectra of an incident wave through a finite structure composed of stepped-changing unit cells (Case 3) is calculated for different frequency regions, shown in Fig. 6. It is interesting to note that the energy of the transmitted wave is significantly reduced when $\Omega < \Omega_c$ even though there is only one unit cell. Apparently, the number of unit cells has no direct relationship with the trapping phenomenon. The rate of energy decay is related to

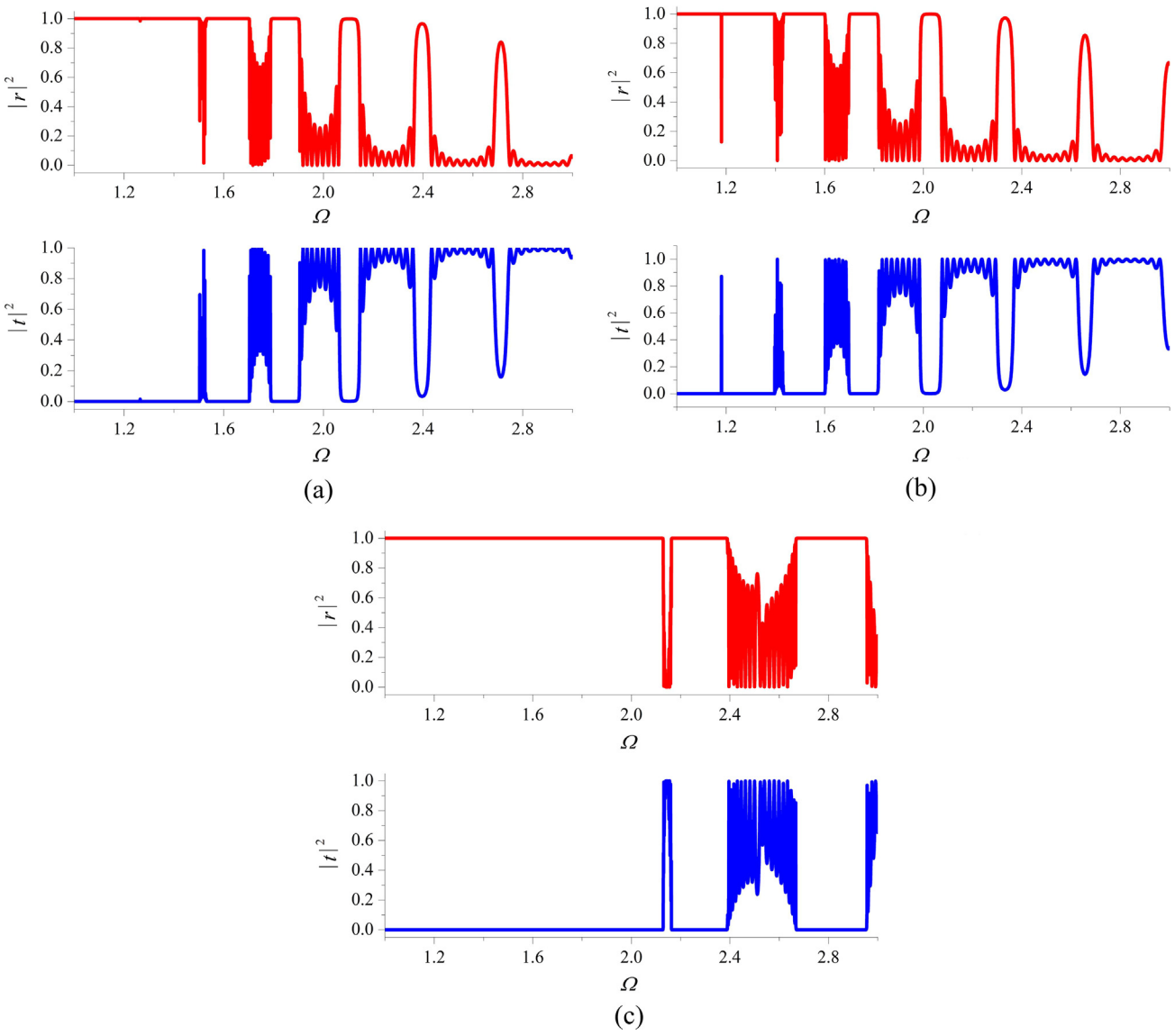

Fig. 4. Reflection and transmission spectra when an incident wave propagates through ten unit cells with thickness changing in the form of: (a) Case 1; (b) Case 2; (c) Case 3.

the length of thinner part and the incident frequency. Smaller Ω and larger b will lead to reduced energy transmission, in agreement with the explanation on the trapped modes mentioned above. For comparison, we also show the transmission coefficient when $\Omega > \Omega_c$ in Fig. 6(b), with N being the number of unit cell defined in Fig. 1(a). In this case, k' is a real number, corresponding to wave propagation without attenuation. The existence of band gap in this frequency region is mainly caused by Bragg scattering effect. The frequency regions, at which the amplitude of incident wave has been neutralized with the reflected wave, finally form the stop band. Larger number of unit cell will promote better wave interactions, leading to more obvious stop band [30,31], as shown in Figs. 6(b) and 4(c).

As a partial conclusion, simulation results revealed two different kinds of physical phenomena for thickness shear waves propagating in periodic quartz plate. When the frequency lies in the region larger than the cut-off frequency, the formation of the band gap is caused by Bragg scattering effect, greatly influenced by the number of unit cells. However, below the cut-off frequency, corresponding to a pure imaginary wavenumber and decaying amplitude, energy trapping takes place, which is insensitive to the structural periodicity. Based on the physical mechanism of trapped modes, we will explore its application in an acoustic wave filter in the following discussions.

4. Thickness shear trapped modes for acoustic wave filter design

The discovery and discussions on the trapped modes offer opportunities for designing various acoustic devices. An example of an acoustic filter is given hereafter, with its thickness changing sectionally along $\pm x_3$ directions, as shown in Fig. 7(a). The thickness of the plate is $2h_0$, $1.8h_0$, $1.6h_0$, $1.4h_0$, $1.2h_0$ and h_0 at $|x_3| \leqslant b$, $b \leqslant |x_3| \leqslant 2b$, $2b \leqslant |x_3| \leqslant 3b$, $3b \leqslant |x_3| \leqslant 4b$, $4b \leqslant |x_3| \leqslant 5b$ and $|x_3| \geqslant 5b$, respectively. Correspondingly, the values of Ω_c in each sub-regions are 1, 1.111, 1.25, 1.429, 1.667 and 2. For simplification, we use Eq. (12) and the transfer matrix method during the following numerical simulation. For FEM simulations, two additional perfect match layers (PMLs) are applied as extended domains at the region $|x_3| \geqslant 5b$ to prevent wave reflections [9,32], shown in Fig. 7(b). We mainly focus on the energy trapping phenomenon

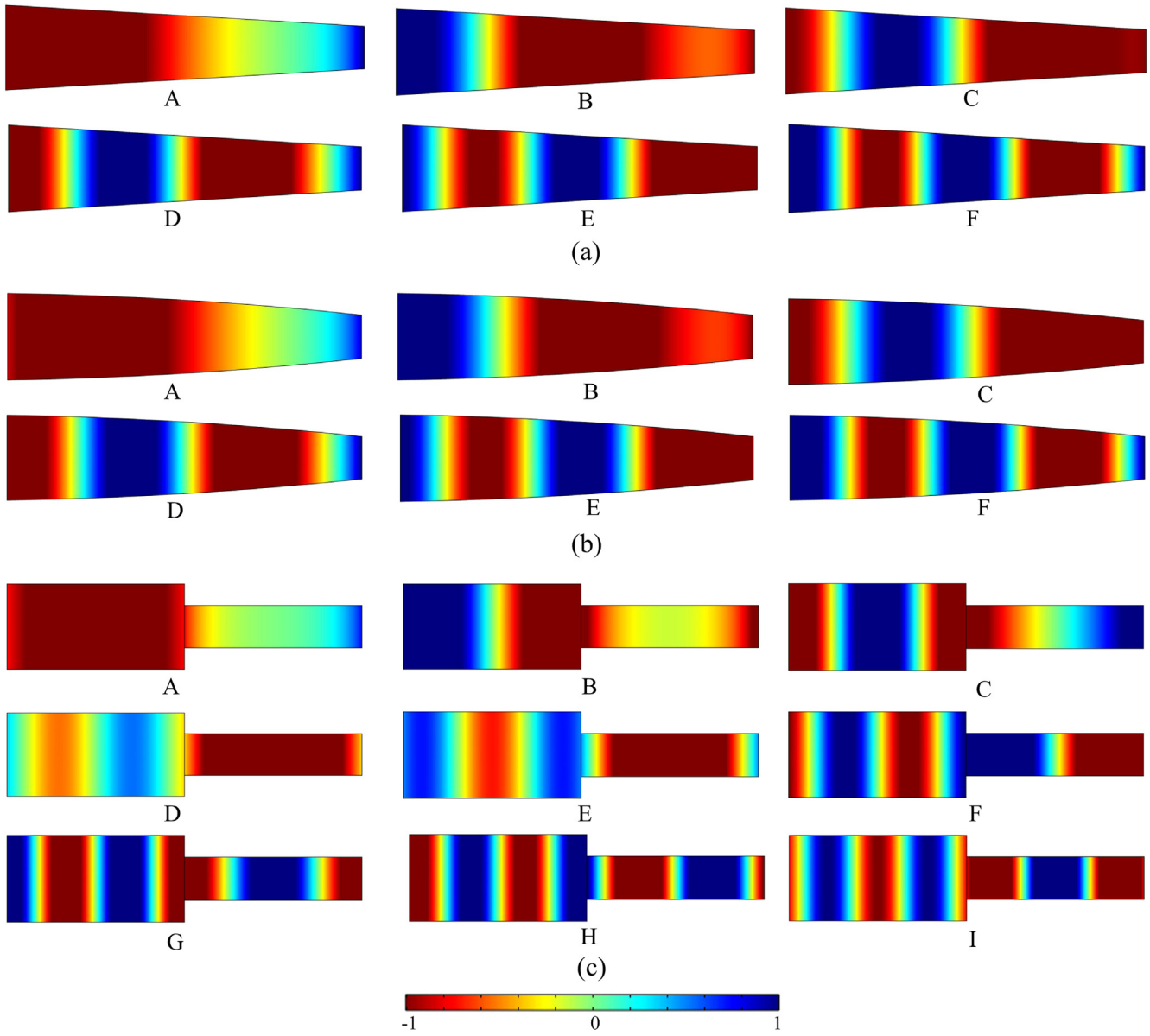

Fig. 5. Displacement field of the modes labeled by capital letters in Fig. 3 for different cases: (a) Case 1; (b) Case 2; (c) Case 3.

caused by thickness changes, so that the non-dimensional frequency will be limited to $1 \leqslant \Omega \leqslant 2$.

For every flat sub-section in the region of $0 \leqslant |x_3| \leqslant 5b$, Eq. (12) is the exact solution for the thickness shear waves. However, for the region of $|x_3| > 5b$, either A' (for $x_3 > 5b$) or B' (for $x_3 < -5b$) is used to describe the amplitude of the outgoing waves. At every interface between each adjacent sub-regions, the continuity of displacement and the moment of shear stress is adopted so that an implicit frequency equation about Ω can be obtained. Fig. 8 shows the variation pattern of Ω of different thickness shear modes existing in the structure designed with the length parameter b. All these frequencies of the thickness shear vibration initiate cut-off frequency of the unbounded quartz plate with thickness of $2h_0$ ($\Omega_c = 2$), and approach the value equalling to $\Omega_c = 1$ with the increasing b. This means the longer embed thinner portion decreases the resonance frequency, with more modes trapped in this region. The effect is the same as that of inertial mass layer, attached on the surface of quartz plate [33]. On the other hand, higher modes appear periodically with the increasing b, which can be seen from Fig. 8. For instance, the second mode appears at $b = 0.26h_0$; the third one at $b = 0.45h_0$; the forth and fifth modes at $b = 0.66h_0$ and $b = 0.85h_0$, respectively. The period Δb is about $0.19h_0$.

Fig. 9 gives the displacement distribution for different trapped modes, marked from A to K in Fig. 8, along x_3 direction when $b = 2h_0$. The amplitude has been normalized such that the displacement of the left- or right-hand-side traveling wave in the center region $|x_3| \leqslant b$ is equal to one. We can see the inner resonance nature of the patterns, with the internal vibrational magnitude of higher modes larger than that in the center region. This phenomenon is in accordance with the work by Cao et al. [30] and Hussein et al. [31]. It can also be concluded from Fig. 8 that, if a thickness shear wave is excited in the central region, i.e., $|x_3| \leqslant b$, the one with higher frequency can propagate longer distance away from the center. Taking Mode E for example, its resonance frequency is $\Omega = 1.5149$, which is located between the two

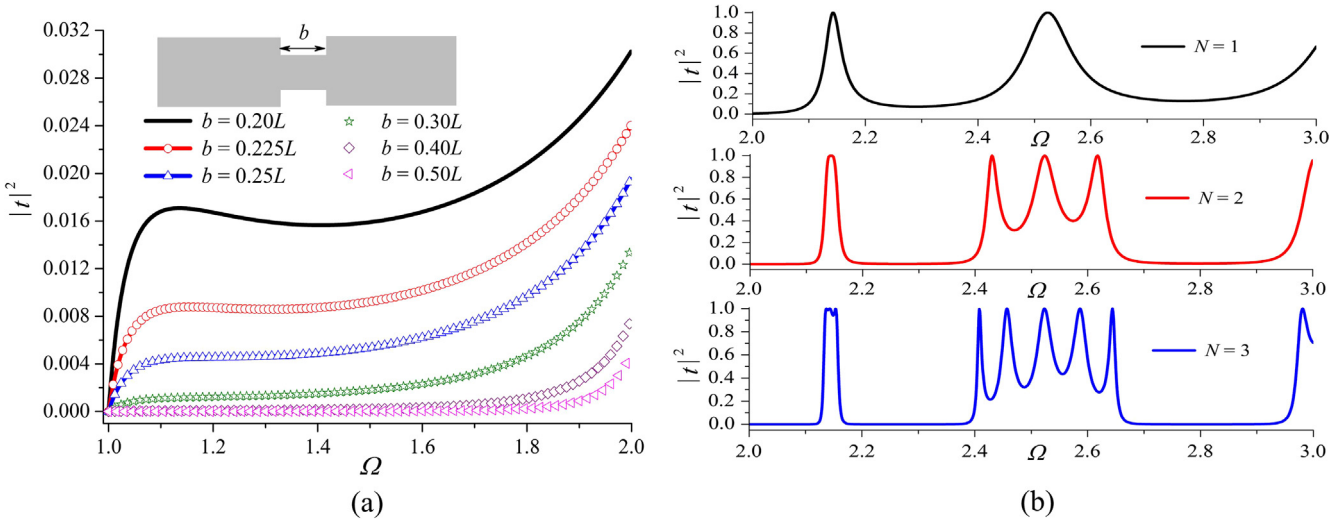

Fig. 6. Transmission coefficient versus incident frequency for different size composites: (a) Ω changing in the region [1,2] with $N = 1$; (b) Ω changing in the region [2,3] for different N.

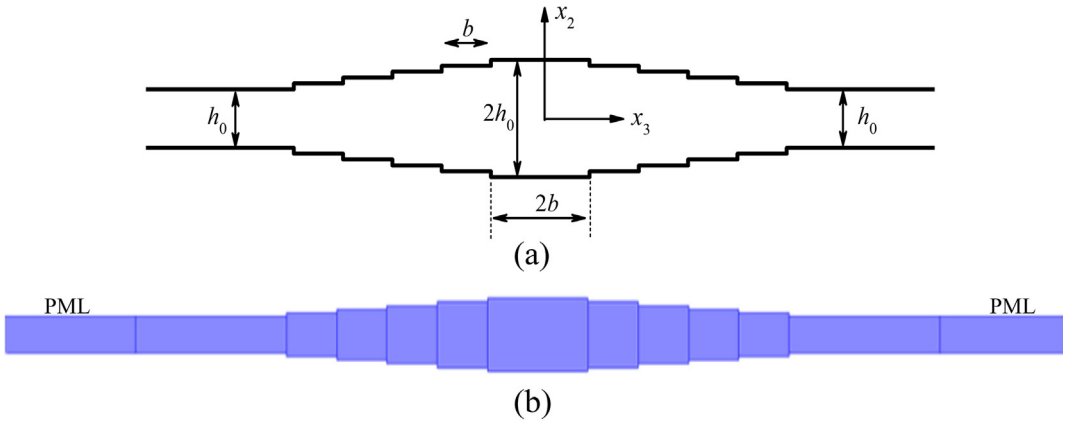

Fig. 7. Acoustic wave filter made of quartz plate with its thickness changing sectionally along $\pm x_3$ direction: (a) theoretical results; (b) FEM results.

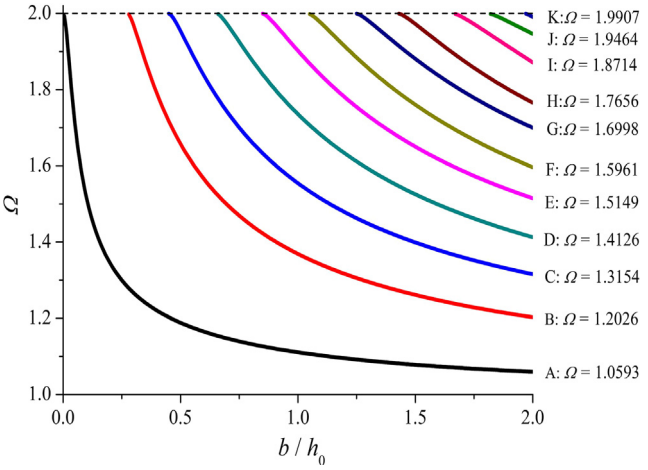

Fig. 8. Non-dimensional frequency Ω of the trapped thickness shear modes for a quartz wave filter with varying length parameter b.

corresponding cut-off frequencies $\Omega_c = 1.4285$ (i.e., the thickness is $1.4h_0$) and $\Omega_c = 1.6667$ (i.e., the thickness is $1.2h_0$). Hence, the wave can be viewed as a propagation wave with its displacement represented by sine and cosine functions in the region $|x_3| \leqslant 4b$. However, when the wave travels in the region $|x_3| \geqslant 4b$, the amplitude decays exponentially during propagation due to the imaginary wavenumber. In contrast, for Mode A, $\Omega = 1.0593$, which is larger than $\Omega_c = 1$ (i.e., the thickness is $2.0h_0$) and smaller than $\Omega_c = 1.111$ (i.e., the thickness is $1.8h_0$), the vibration is reduced evidently only after the wave arrives at $|x_3| = b$. Other waves in Fig. 9 behave similarly. The displacements of Mode J and K do not decay to zero at $|x_3| = 8b$ because higher frequencies lead to slower decaying rate, as shown in Fig. 6(a). As comparison with Fig. 9, Fig. 10 gives the displacement distribution of different trapped modes exported by FEM under the same condition. A slight difference in the resonance frequencies calculated by FEM and theoretical analysis exists, which again is attributed to the application of an equivalent continuity of shear stress moment during theoretical treatment. Nevertheless, the energy trapping phenomenon in Fig. 10 is basically identical as shown in Fig. 9.

It is relevant to note that, although similar phenomenon can also be achieved through Bragg scattering effect [32], the quantitative relationship between the frequency and various structural intrinsic parameters is difficult to established and realized. In present case, however, the simple quantitative relation between the frequency and thickness can be obtained through the concept of cut-off frequency based on the proposed model.

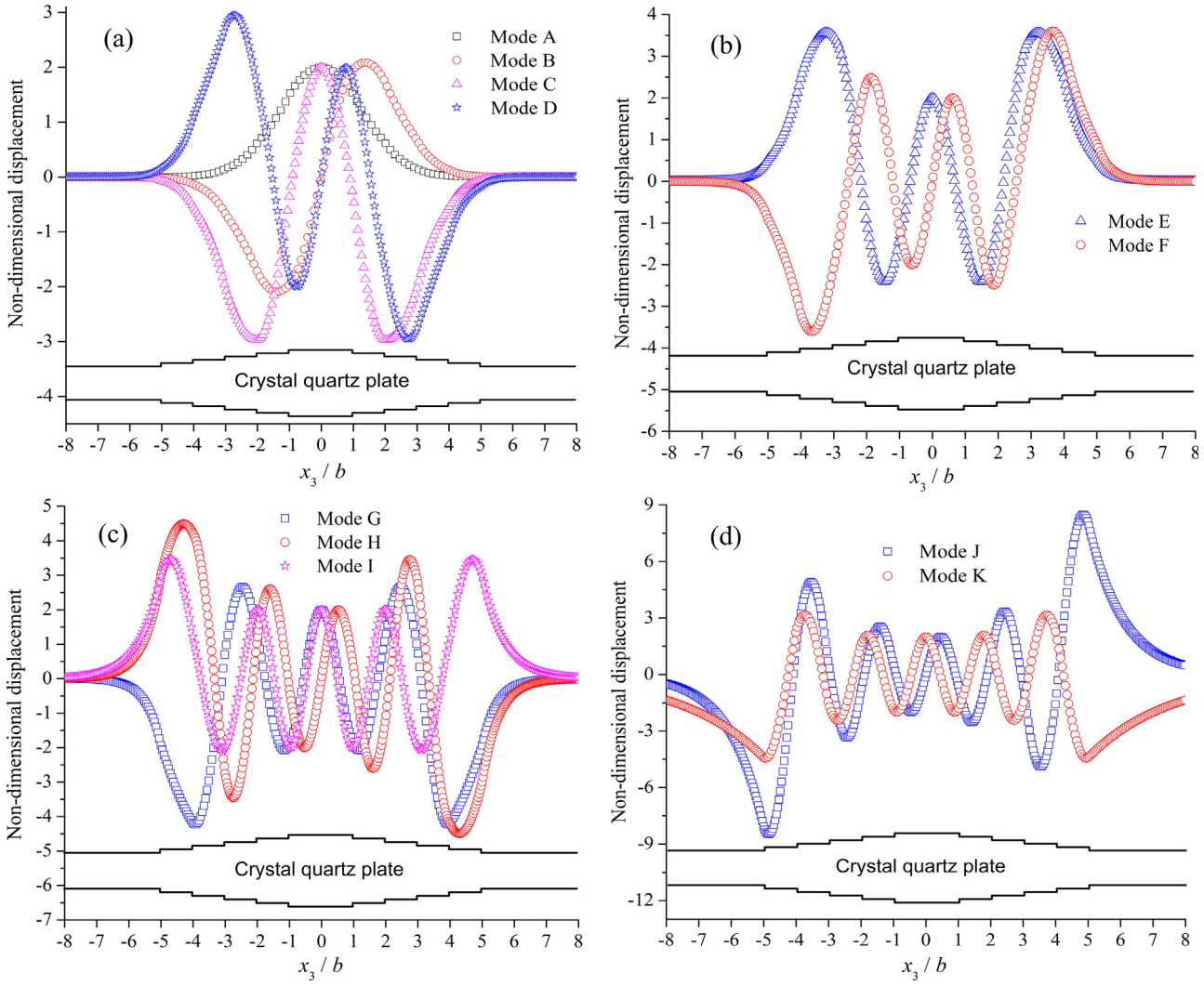

Fig. 9. Non-dimensional displacement distribution of different modes marked in Fig. 8 along x_3 direction ($b = 2h_0$) by the present model: (a) Modes A, B, C and D; (b) Modes E and F; (c) Modes G, H and I; (d) Modes J and K.

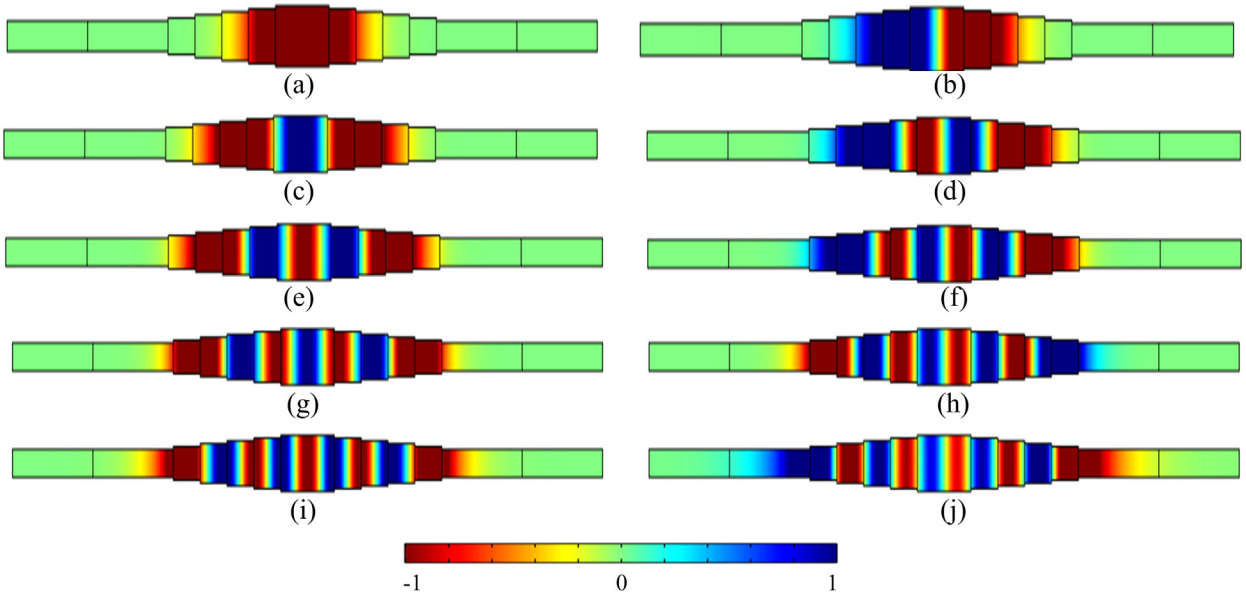

Fig. 10. Non-dimensional displacement distribution of different modes along x_3 direction by FEM ($b = 2h_0$): (a) $\Omega = 1.0645$; (b) $\Omega = 1.2049$; (c) $\Omega = 1.3174$; (d) $\Omega = 1.4165$; (e) $\Omega = 1.5167$; (f) $\Omega = 1.6028$; (g) $\Omega = 1.7009$; (h) $\Omega = 1.7755$; (i) $\Omega = 1.8741$; (j) $\Omega = 1.9511$.

5. Conclusions

In this paper, thickness shear wave propagation in an inhomogeneous quartz plate with periodically changing thickness is investigated. Through power series expansion, a theoretical model, along with the solving procedure, is established. The proposed model is capable of handling various thickness profiles which can be mathematically defined. Numerical studies on typical thickness profiles allow the determination of the dispersion curves and the disclosure of the resonant trapped modes. The trapped modes are dominated by the plate thickness, delimited by the so-called cut-off frequency which increases with reducing plate thickness. Two mechanisms behind the formation of the band gap are confirmed. When the frequency of the wave exceeds the cut-off frequency, Bragg scattering dominates the process with strong dependence on the number of the unit cells; below the cut-off frequency, however, energy trapping takes place, irrespective of the structural periodicity and number of cells. To explore the phenomenon, application of the thickness shear trapped modes in an acoustic wave filter is demonstrated, in which the waves with different frequencies can be trapped in different regions. Results allow better understanding on the trapped thickness shear wave behaviors, and point to the possibility of conceiving efficient and tunable acoustic wave filters.

Acknowledgment

This work was supported by the National Natural Science Foundation of China (No. 11402187), Hong Kong Scholars Program (XJ2015039), Project Funded by China Postdoctoral Science Foundation (2014M560762) and Fundamental Research Funds for the Central Universities of China.

References

[1] M.S. Kushwaha, P. Halevi, L. Dobrzynski, B. Djafari-Rouhani, Acoustic band structure of periodic elastic composites, Phys. Rev. Lett. 71 (1993) 2022–2025.
[2] X. Guo, P. Wei, M. Lan, L. Li, Dispersion relations of elastic waves in one-dimensional piezoelectric/piezomagnetic phononic crystal with functionally graded interlayers, Ultrasonics 70 (2016) 158–171.
[3] Z.Y. Liu, X.X. Zhang, Y.W. Mao, Y.Y. Zhu, Z.Y. Yang, C.T. Chan, P. Sheng, Locally resonant sonic materials, Science 289 (2000) 1734–1736.
[4] M. Hirsekorn, P.P. Delsanto, A.C. Leung, P. Matic, Elastic wave propagation in locally resonant sonic material: comparison between local interaction simulation approach and modal analysis, J. Appl. Phys. 99 (2006) 124912.
[5] Y. Pennec, B. Djafari-Rouhani, H. Larabi, J.O. Vasseur, A.C. Hladky-Hennion, Low-frequency gaps in a phononic crystal constituted of cylindrical dots deposited on a thin homogeneous plate, Phys. Rev. B 78 (2008) 104105.
[6] H. Larabi, Y. Pennec, B. Djafari-Rouhani, J.O. Vasseur, Multicoaxial cylindrical inclusions in locally resonant phononic crystals, Phys. Rev. E 75 (2007) 066601.
[7] M. Oudich, M. Senesi, M. Badreddine Assouar, M. Ruzenne, J.H. Sun, B. Vincent, Experimental evidence of locally resonant sonic band gap in two-dimensional phononic stubbed plates, Phys. Rev. B 84 (2011) 165136.
[8] A. Khelif, B. Aoubiza, S. Mohammadi, A. Adibi, V. Laude, Complete band gaps in two-dimensional phononic crystal slabs, Phys. Rev. E 74 (2006) 046610.
[9] S. Banerjee, T. Kundu, Elastic wave propagation in sinusoidally corrugated waveguides, J. Acoust. Soc. Am. 119 (2006) 2006–2017.
[10] G. Trainiti, J.J. Rimoli, M. Ruzzene, Wave propagation in periodically undulated beams and plates, Int. J. Solids Struct. 75–76 (2015) 260–276.
[11] A. Boström, Acoustic waves in a cylindrical duct with periodically varying cross section, Wave Motion 5 (1983) 59–67.
[12] M. Bavencoffe, B. Morvan, A.-C. Hladky-Hennion, J.-L. Izbicki, Experimental and numerical study of evanescent waves in the mini stopband of a 1D phononic crystal, Ultrasonics 53 (2013) 313–319.
[13] S.E. Sandström, Stopbands in a corrugated parallel plate waveguide, J. Acoust. Soc. Am. 79 (1986) 1293–1298.
[14] V.S. Sorokin, Effects of corrugation shape on frequency band-gaps for longitudinal wave motion in a periodic elastic layer, J. Acoust. Soc. Am. 139 (2016) 1898–1908.
[15] A. Climente, D. Torrent, J. Sanchez-Dehesa, Gradient index lenses for flexural waves based on thickness variations, Appl. Phys. Lett. 105 (2014) 064101.
[16] J. Zhu, W.Q. Chen, J.S. Yang, Propagation of thickness-twist waves in elastic plates with periodically varying thickness and phononic crystals, Ultrasonics 54 (2014) 1899–1903.
[17] Y.L. Xu, Analytical study of dispersion relations for shear horizontal wave propagation in plates with periodic stubs, Ultrasonics 61 (2015) 114–120.
[18] H.F. Zhu, F. Semperlotti, Phononic thin plates with embedded acoustic black holes, Phys. Rev. B 91 (2015) 104304.
[19] W.Y. Wang, C. Zhang, Z.T. Zhang, T.F. Ma, G.P. Feng, Energy-trapping mode in lateral-field-excited acoustic wave devices, Appl. Phys. Lett. 94 (2009) 192901.
[20] P.J. Cumpson, M.P. Seah, The quartz crystal microbalance: radial/polar dependence of mass sensitivity both on and off the electrodes, Meas. Sci. Technol. 1 (1990) 544–555.
[21] P. Li, F. Jin, J.S. Yang, Thickness-shear vibration of an AT-cut quartz resonator with a hyperbolic contour, IEEE Trans. Ultrason., Ferroelect., Freq. Contr. 59 (2012) 1006–1012.
[22] Z.N. Zhao, Z.H. Qian, B. Wang, Energy trapping of thickness-extensional modes in thin film bulk acoustic wave filters, AIP Adv. 6 (2016) 015002.
[23] H.F. Tiersten, Analysis of trapped-energy resonators operating in overtones of coupled thickness shear and thickness twist, J. Acoust. Soc. Am. 59 (1976) 879–888.
[24] W.J. Wang, R.X. Wu, J. Wang, J.K. Du, J.S. Yang, Thickness-shear modes of an elliptical, contoured AT-cut quartz resonator, IEEE Trans. Ultrason. Ferroelect. Freq. Contr. 60 (2013) 1192–1198.
[25] Z.N. Zhao, Z.H. Qian, B. Wang, J.S. Yang, Thickness-shear and thickness-twist modes in an AT-cut quartz acoustic wave filter, Ultrasonics 58 (2015) 1–5.
[26] H.F. Tiersten, R.C. Smythe, An analysis of contoured crystal resonators operating in overtones of coupled thickness shear and thickness twist, J. Acoust. Soc. Am. 65 (1979) 1455–1460.
[27] X.S. Cao, F. Jin, I. Jeon, Calculation of propagation properties of Lamb waves in a functionally graded material (FGM) plate by power series technique, NDT&E Int. 44 (2011) 84–92.
[28] S.I. Fomenko, M.V. Golub, Ch. Zhang, T.Q. Bui, Y.S. Wang, In-plane elastic wave propagation and band-gaps in layered functionally graded phononic crystals, Int. J. Solids Struct. 51 (2014) 2491–2503.
[29] G. Johansson, A.J. Niklasson, Approximate dynamic boundary conditions for a thin piezoelectric layer, Int. J. Solids Struct. 40 (2003) 3477–3492.
[30] W.W. Cao, W.K. Qi, Plane wave propagation in finite 2–2 composites, J. Appl. Phys. 78 (1995) 4627–4632.
[31] M.I. Hussein, G.M. Hulbert, R.A. Scott, Dispersive elastodynamics of 1D banded materials and structures: analysis, J. Sound Vib. 289 (2006) 779–806.
[32] Y.L. Xu, Spatial bandwidth enlargement and field enhancement of shear horizontal waves in finite graded piezoelectric layered media, Phys. Lett. A 379 (2015) 1752–1756.
[33] P. Li, F. Jin, The anti-plane vibration of a quartz plate with an additional partial non-uniform mass layer for acoustic wave sensing, Acta Mech. 224 (2013) 1397–1414.